Volume 10
Number 23
21 June 2022
Pages 4323–4520

Journal of Materials Chemistry B

Materials for biology and medicine

rsc.li/materials-b

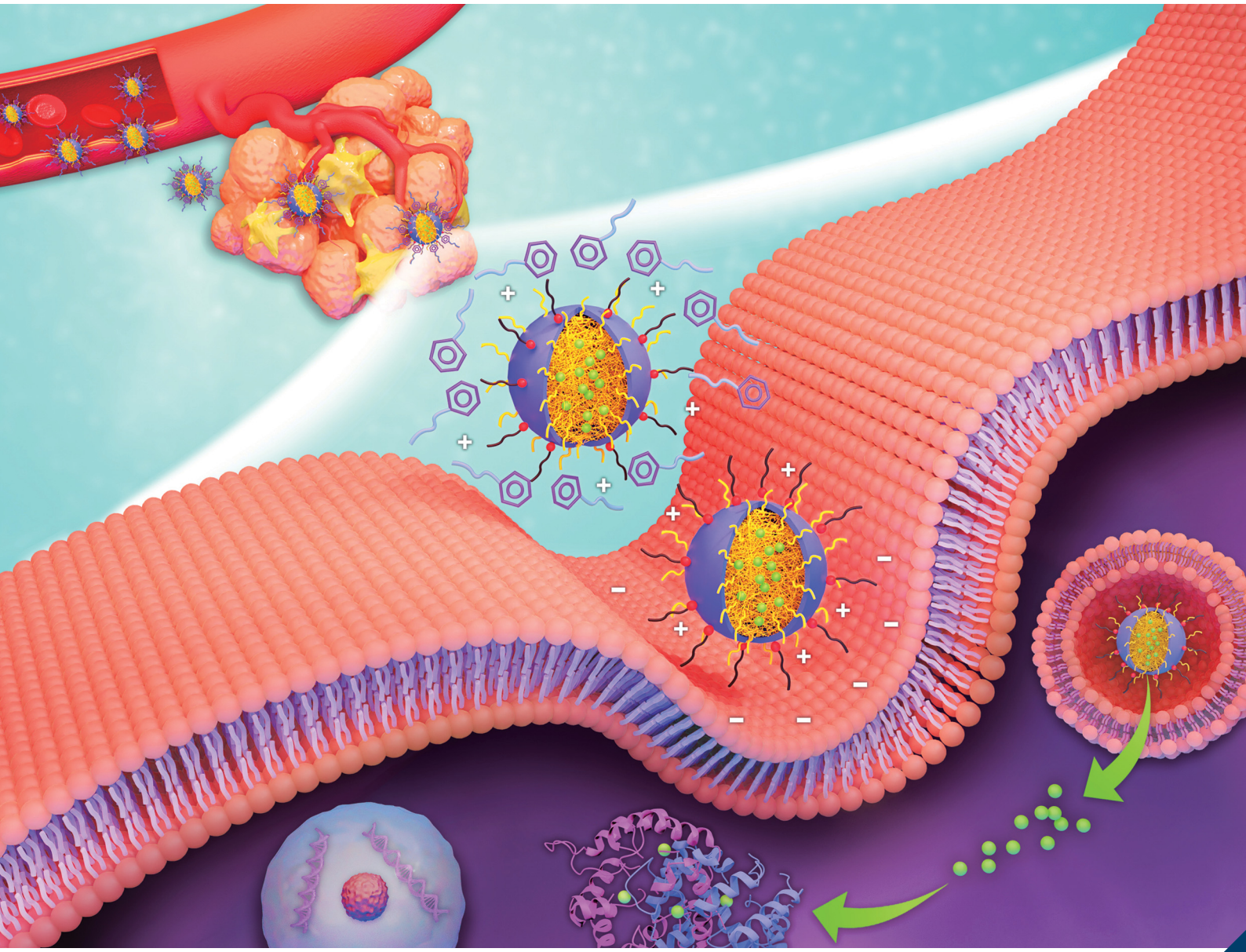

ISSN 2050-750X

PAPER

Bor-Show Tzang, Wen-Hsuan Chiang *et al.*
Tumor acidity-responsive polymeric nanoparticles to promote intracellular delivery of zoledronic acid by PEG detachment and positive charge exposure for enhanced antitumor potency

ROYAL SOCIETY OF CHEMISTRY

Indexed in Medline!

Journal of Materials Chemistry B

ROYAL SOCIETY OF CHEMISTRY

PAPER

View Article Online
View Journal | View Issue

Published on 29 April 2022. Downloaded by National Chung Hsing University on 6/16/2022 2:37:46 AM.

Check for updates

Cite this: *J. Mater. Chem. B*, 2022, **10**, 4363

Tumor acidity-responsive polymeric nanoparticles to promote intracellular delivery of zoledronic acid by PEG detachment and positive charge exposure for enhanced antitumor potency†

Ya-Hsuan Chou,[a] Yu-Ling Liu,[a] Tsai-Ching Hsu,[bcd] Jia-Le Yow,[b] Bor-Show Tzang*[bcde] and Wen-Hsuan Chiang*[a]

Received 30th March 2022,
Accepted 29th April 2022

DOI: 10.1039/d2tb00695b

rsc.li/materials-b

Zoledronic acid (ZA), a third-generation bisphosphonate, has been extensively used to treat osteoporosis and cancer bone metastasis and demonstrated to suppress proliferation of varied cancer cells and selectively kill tumor-associated microphages (TAMs). However, the clinical applications of ZA in extraskeletal tumor treatment are largely restricted due to its rapid renal clearance and binding to bones. In this study, to promote intracellular delivery of ZA for amplified antitumor efficacy, tumor acidity-responsive polymeric nanoparticles with high ZA payload (*ca.* 12.3 wt%) and low premature ZA leakage were designed. As a pivotal material for surface coating, the acidity-sensitive and amphiphilic methoxy poly(ethylene glycol) (mPEG)-benzoic imine-octadecane (C18) (mPEG-*b*-C18) was synthesized by conjugation of mPEG-CHO with 1-octadecylamine upon Schiff base reaction. Through tailor-made co-assembly of the hydrophobic poly(lactic-*co*-glycolic acid) (PLGA), amphiphilic tocopheryl polyethylene glycol succinate (TPGS) and mPEG-*b*-C18 to encapsulate ionic complexes composed of ZA molecules and branched poly(ethylenimine) (PEI) segments, the attained therapeutic polymeric nanoparticles, characterized to have a hydrophobic PLGA/ZA/PEI-constituted core covered with mPEG-*b*-C18 and TPGS, were able to not only detach mPEG shielding upon acidity-triggered hydrolysis of benzoic imine bonds but also expose surface positive charges of protonated PEI segments. The *in vitro* cellular uptake and cytotoxicity studies demonstrated that the internalization of acidity-sensitive ZA-encapsulated nanoparticles by TRAMP-C1 mouse prostate cancer cells and murine macrophages RAW 264.7 was considerably promoted upon acidity-elicited PEG detachment and surface charge conversion, thus remarkably boosting intracellular ZA delivery and anticancer potency. Compared to PEG non-detachable ZA-loaded nanoparticles with poor tumor deposition and antitumor effect, the PEG-detachable ZA-carrying nanoparticles markedly accumulated in TRAMP-C1 solid tumors *in vivo* and inhibited tumor growth, thereby increasing the survival rate of the treated mice. The collective data suggest the great promise of tumor acidity-sensitive ZA-carrying hybrid nanoparticles in the treatment of extraskeletal solid tumors.

1. Introduction

Bisphosphonates, a kind of small molecular drug, have been extensively utilized to treat cancer bone metastasis and osteoporosis of postmenopausal women due to their bone-homing capability and stability.[1–3] Zoledronic acid (ZA), a third-generation bisphosphonate, has been demonstrated to suppress osteolysis and prevent breast cancer bone metastasis.[3–7] Also, some studies have shown that ZA can reduce cell migration and proliferation by inhibiting farnesyl diphosphate synthase (FPPS), a key enzyme of the mevalonate route.[8–10] Increasing findings have highlighted that ZA can selectively kill tumor-associated microphages (TAMs) in the tumor microenvironment.[11,12] Despite

[a] *Department of Chemical Engineering, National Chung Hsing University, Taichung 402, Taiwan. E-mail: whchiang@dragon.nchu.edu.tw*
[b] *Institute of Medicine, Chung Shan Medical University, Taichung 402, Taiwan. E-mail: bstzang@csmu.edu.tw*
[c] *Clinical Laboratory, Chung Shan Medical University Hospital, Taichung 402, Taiwan*
[d] *Immunology Research Center, Chung Shan Medical University, Taichung 402, Taiwan*
[e] *Department of Biochemistry, School of Medicine, Chung Shan Medical University, Taichung 402, Taiwan*

† Electronic supplementary information (ESI) available. See DOI: https://doi.org/10.1039/d2tb00695b

Published on 29 April 2022. Downloaded by National Chung Hsing University on 6/16/2022 2:37:46 AM.

the great potential of ZA in cancer treatment, several drawbacks of ZA including short blood circulation half-life (105 min), relatively low maximum plasma concentration (*ca.* 1 μM), and massive adsorption by the bone tissues (*ca.* 55% of intravenously-injected ZA) considerably limited its clinical use as a therapeutic agent for treatment of extraskeletal solid tumors.[13,14]

Recently, to enhance the accumulation of ZA in extraskeletal tumors for improved antitumor efficacy, a variety of nanoparticles such as liposomes,[15,16] polymeric nanoparticles,[17–19] lipid-coated nanoparticles[11] and ceramic-based nanoparticles[20–22] have been developed as vehicles for ZA molecules. Generally, the encapsulation of ZA into the above nanoparticles increased its cytotoxicity toward cancer cells and antitumor potency in animal models by partly reduced adsorption of ZA in bone sites. Unfortunately, many of these ZA-carrying nanoparticles exhibited low ZA loading capability and significant premature ZA leakage in a physiological environment, thereby appreciably declining their antitumor effect. For example, for ZA-loaded liposomes,[15,16] the ZA loading content was below 10 wt%. Khajuria and co-workers found that beyond 60% of ZA was liberated from ZA-loaded hydroxyapatite-based nanoparticles within 60 min.[21] Furthermore, despite the effective treatment of ZA-conjugated gold nanorod-enclosed mesoporous silica nanoparticles for breast cancer bone metastasis,[3] considerable ZA release (more than 60% during 5 h) was observed.

In order to promote ZA accumulation within extraskeletal solid tumors, some functionalized ZA-carrying nanoparticles were equipped with lowered premature ZA release and hydrophilic PEG-modified surfaces.[14,19,23] The PEGylation of nanovehicles could prolong their blood circulation time upon reducing the uptake by the reticuloendothelial system, but remarkably hinder their cellular internalization and tumor accumulation, thus being not beneficial for tumor-targeted drug delivery.[24–26] To enhance the affinity between nanoparticles and cancer cells, new strategies of engineering ZA-loaded nanoparticles with a detachable PEG shield in response to weak acidity (pH 6.2–6.9) of the tumor microenvironment have emerged.[11,18] Cui's group reported that the ZA/calcium complex-enclosed PLGA nanoparticles emulsified with octadecanoic acid–hydrazine–PEG remarkably decreased the distribution of ZA in bones and enhanced its deposition in extraskeletal tumors in mice with orthotopically implanted mammary tumors by acid-sensitive detachable PEGylation.[18] In a similar way, for selectively killing TAMs in the tumor microenvironment, lipid-coated ZA/calcium complexes modified with mannose and an acid-labile PEG shell were designed by Chen and co-workers.[11] *In vivo* biodistribution and antitumor studies proved that these ZA-loaded nanoparticles effectively accumulated in tumors and eliminated TAMs, thereby considerably suppressing tumor growth. Despite the decreased premature drug leakage and promoted intracellular drug delivery of the aforementioned PEG detachable ZA-carrying nanoparticles, their drug loading content was still less than 3.0 wt%. Note that, in addition to acidity-elicited dePEGylation, the surface charge conversion of nanocarriers in an acidic tumor microenvironment from negative to neutral/positive has been demonstrated to prominently promote their cellular uptake and tumor accumulation.[27,28]

To boost the antitumor efficacy of ZA by minimizing premature drug leakage and achieving effective intracellular drug delivery, tailor-made hybrid polymeric nanoparticles capable of carrying high ZA payload, shedding the PEG shield and then exposing surface positive charges in response to an acidic tumor microenvironment were designed herein. To the best of our knowledge, the development of ZA-encapsulated nanoparticles equipped with dual pH-triggered PEG detachment and surface charge conversion has never been reported. First, the acidity-sensitive and amphiphilic methoxy-PEG (mPEG)-benzoic imine-octadecane (C18) (mPEG-*b*-C18) segments utilized as a crucial material for surface coating were synthesized by conjugation of mPEG-CHO with 1-octadecylamine upon Schiff base reaction. Through hydrophobic co-anchoring of amphiphilic mPEG-*b*-C18 and tocopheryl polyethylene glycol succinate (TPGS) on the surfaces of a PLGA-rich core enclosing ZA/poly(ethylenimine) (PEI) ionic complexes, hybrid nanoparticles with high ZA payload (*ca.* 12.3 wt%) were attained (Scheme 1). The ZA/PEI-encapsulated hybrid nanoparticles showed not only low ZA leakage under physiology mimicking conditions, but also superior colloidal stability in serum-containing aqueous solution. Notably, due to dePEGylation upon acid-triggered hydrolysis of benzoic imine bonds and exposure of surface positive charges from protonated PEI segments, these therapeutic hybrid nanoparticles were remarkably internalized by TRAMP-C1 prostate cancer cells and macrophage-like RAW 264.7 cells, thus considerably promoting the ZA-mediated cytotoxicity. The preliminary results of *in vivo* animal studies showed that the tumor acidity-responsive ZA-carrying hybrid nanoparticles appreciably hindered TRAMP-C1 tumor growth and prolonged the median survival of treated mice, demonstrating superior activity to free ZA molecules and

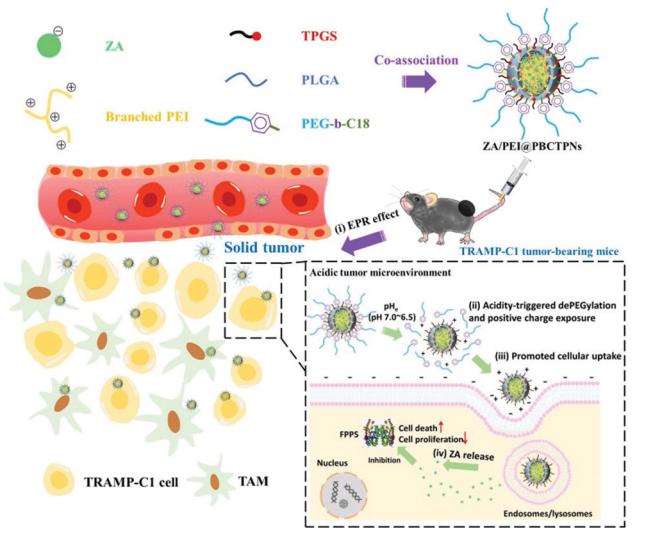

Scheme 1 Illustration of promoted intratumoral accumulation and cellular uptake of tumor acidity-responsive ZA-carrying hybrid nanoparticles upon acid-triggered PEG detachment and positive charge exposure to enhance antitumor efficacy.

This journal is © The Royal Society of Chemistry 2022

Published on 29 April 2022. Downloaded by National Chung Hsing University on 6/16/2022 2:37:46 AM.

ZA-loaded nanoparticles lacking acid sensitivity. These findings suggest the great potential of tumor acidity-responsive ZA-carrying hybrid nanoparticles in the treatment of extraskeletal solid tumors.

2. Experimental section

2.1. Materials

ZA was acquired from Tokyo Chemical Industry, Co., Ltd (Japan). PLGA (LA/GA: 75/25, I.V. 0.18 dl g^{-1}, hydroxyl terminated) was purchased from Green Square (Taiwan). Branched PEI (M.W. = 1.8 kDa), *N*,*N*′-dicyclohexylcarbodiimide (DCC, 99%) and 1-octadecylamine (97%) were obtained from Alfa Aesar (USA). Poly(ethylene glycol)methyl ether (mPEG-OH, average M_n 5000), Dulbecco's modified Eagle medium, (DMEM, high glucose 4500 mg mL^{-1}), Hoechst 33342 (>98%), RPMI-1640 medium and $CDCl_3$ (99.8 atom% D) were purchased from Sigma-Aldrich (USA). 4-Dimethylaminopyridine (DMAP, 98%) and 4-formylbenzoic acid (FBA, 95+%) were obtained from Matrix Scientific. Stearic acid was obtained from Acros Organics. TPGS was obtained from Carbosynth Ltd (UK). Fetal bovine serum (FBS) was purchased from Hyclone (USA). 3-(4,5-Dimethylthiazol-2-yl)-2,5-diphenyltetrazolium bromide (MTT) was obtained from ALPHA BIOCHEMSTRY (Taiwan). Deionized water was produced from Milli-Q Synthesis (18 MΩ, Millipore). All other chemicals were of reagent grade and used as received. TRAMP-C1 (mouse prostate cancer cell line), HeLa (human cervical cancer cell line) and macrophage-like RAW264.7 cells were obtained from the Food Industry Research and Development Institute (Hsinchu City, Taiwan).

2.2. Synthesis and characterization of mPEG-*b*-C18 and mPEG-C18 adducts

The mPEG-CHO utilized in this work was prepared using our previous approach.[29] Through the formation of a benzoic imine bond from the Schiff base reaction of mPEG-CHO and 1-octadecylamine, mPEG-*b*-C18 was synthesized (Scheme 2a).[30] Briefly, mPEG-CHO (500 mg), 1-octadecanamine (80 mg) and DMAP (61 mg) were dissolved in dichloromethane (DCM) (5.0 mL). The reaction was carried out under stirring at room temperature for 36 h, followed by the removal of DCM under reduced pressure. Next, the product was collected by precipitation from cold diethyl ether and then dried under vacuum at room temperature overnight. For comparison, the mPEG-C18 without a benzoic imine bond was attained by esterification of mPEG with stearic acid (Scheme 2b). mPEG (1 g), stearic acid (0.29 g), DCC (0.206 g) and DMAP (0.012 g) were dissolved in DCM (5.0 mL). The reaction was performed under stirring at 25 °C for 24 h, followed by elimination of dicyclohexylcarbodiurea by filtration. After concentration of the solution under reduced pressure, the product was then collected by precipitation from cold diethyl ether and dried under vacuum overnight. The compositions of mPEG-*b*-C18 and mPEG-C18 adducts were determined by ^{1}H-NMR spectroscopy (Agilent DD2 600 MHz NMR spectrometer) using $CDCl_3$ as the solvent.

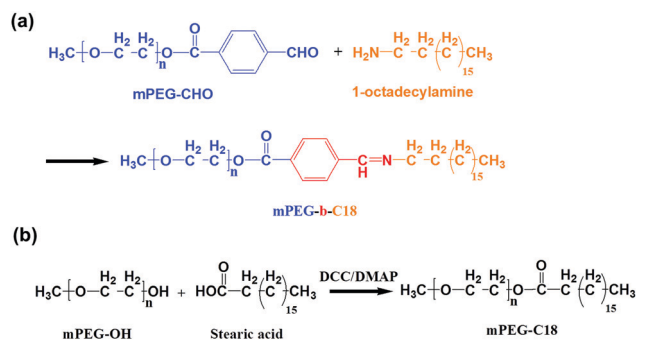

Scheme 2 Synthetic route and chemical structure of (a) mPEG-*b*-C18 and (b) mPEG-C18 adducts.

2.3. Preparation of ZA-carrying hybrid polymeric nanoparticles

The ZA-free and ZA-carrying hybrid polymeric nanoparticles were fabricated using a single-step nanoprecipitation method. The ZA/PEI-encapsulated mPEG-*b*-C18/TPGS/PLGA nanoparticles (hereinafter referred to as ZA/PEI@PBCTPNs) were prepared as follows. First, ZA (3.2 mg) and branched PEI (4.6 mg) were dissolved in tris buffer of pH 8.5 and 6.0 (0.8 mL), respectively. Subsequently, the ZA solution was added into the PEI solution and stirred for 30 min to obtain the ZA/PEI mixtures. The ratio of the number of amines from PEI to the number of phosphonates from ZA (N/P ratio) was fixed at 9.0. TPGS (1.0 mg) in pH 7.4 tris buffer (0.1 mL) was added dropwise to the ZA/PEI mixtures under stirring. Then PLGA (6.0 mg) and mPEG-*b*-C18 (3.0 mg) dissolved in DMSO (0.3 mL) were added to the ZA/PEI/TPGS-containing aqueous solution (1.7 mL) under stirring. The solution was mildly stirred at 25 °C for 60 min and then equilibrated for 1 h. The attained ZA/PEI@PBCTPN suspension was dialyzed (Cellu Sep MWCO 12 000–14 000) with pH 8.0 phosphate buffer (10 mM) at 4 °C to eliminate DMSO and unloaded ZA. For comparison, the ZA@PBCTPNs without PEI addition, ZA/PEI@PBCTPNs (4.5) with an N/P ratio of 4.5, ZA/PEI-loaded mPEG-C18/TPGS/PLGA nanoparticles (ZA/PEI@PCTPNs) (9.0) with an N/P ratio of 9.0 and drug-free PEI@PBCTPNs were also obtained in a similar way.

2.4. Characterization of various ZA-encapsulated hybrid polymeric nanoparticles

The particle size and size distribution (polydispersity index, PDI) of ZA-carrying hybrid polymeric nanoparticles in aqueous solutions were determined by a Brookhaven BI-200SM goniometer equipped with a BI-9000 AT digital correlator using a solid-state laser (35 mW, λ = 637 nm) detected at a scattering angle of 90°. The data shown herein represent an average of at least triplicate measurements. Moreover, the angular dependence of the autocorrelation functions of various hybrid polymeric nanoparticles was evaluated with the above apparatus. Correlation functions were obtained by the cumulant method at different angles. The zeta potential of various hybrid nanoparticles in aqueous solutions was examined using a Litesizer

Published on 29 April 2022. Downloaded by National Chung Hsing University on 6/16/2022 2:37:46 AM.

500 (Anton Paar, USA). The morphology of ZA-encapsulated hybrid nanoparticles negatively stained with 2 wt% phosphotungstic acid hydrate was observed using a transmission electron microscope (TEM) (JEOL JEM-1400 CXII microscope).

To quantify ZA loaded within hybrid nanoparticles, a prescribed volume of ZA-carrying nanoparticle suspension was freeze-dried and then dispersed in DMSO to disrupt the colloidal structure and allow ZA precipitation. The ZA precipitate was collected by centrifugation and then freeze-dried. After complete dissolution of ZA pellets in deionized water, the ZA concentration was measured by ThermoFisher high-performance liquid chromatography (HPLC) with a reversed-phase C18 column (4.6 × 250 mm and 5 mm, Sigma-Aldrich (USA)). The mobile phase consisted of aqueous orthophosphoric acid solution (pH 6.0) and acetonitrile (88 : 12, v/v) with a gradient elution pumped at a flow rate of 1.0 mL min^{-1}, and the temperature of the column was kept at 27 °C. The absorbance of ZA at 215 nm was determined. The data presented herein represent an average of triplicate measurements. The drug loading efficiency (DLE) and drug loading content (DLC) were calculated using the following formulas:

$$\text{DLE (\%)} = (\text{weight of ZA loaded/weight of ZA in feed}) \times 100\%.$$

$$\text{DLC (\%)} = (\text{weight of ZA loaded/total weight of ZA-containing hybrid nanoparticles}) \times 100\%.$$

2.5. *In vitro* ZA release profiles

For ZA release evaluation, the ZA/PEI@PBCTPN dispersion (1.0 mL) was dialyzed (Cellu Sep MWCO 12 000–14 000) against phosphate buffered saline (PBS) of pH 7.4, 6.5 and 5.0 (ionic strength 0.15 M, 20 mL), respectively, at 37 °C. At different time intervals, 1.0 mL of dialysate (pH 5.0, 6.5 or 7.4) was withdrawn for analysis and replaced with an equivalent volume of fresh medium. The ZA concentration was measured by HPLC as described above.

2.6. *In vitro* cellular uptake

In order to observe the cellular uptake of ZA/PEI@PBCTPNs and ZA/PEI@PCTPNs by fluorescence imaging, the hydrophobic DiO fluorescent dye was encapsulated into these nanoparticles. The DiO-labeled hybrid nanoparticles were first dispersed in PBS of pH 6.5 (regarded as with acid pretreatment) and 7.4 (without acid pretreatment) at 37 °C for 3 h. Subsequently, the attained solutions containing either DiO-encapsulated ZA/PEI@PBCTPNs or ZA/PEI@PCTPNs were diluted with cell culture medium to a DiO concentration of 0.6 μM. TRAMP-C1 cells (2×10^5 cells per well) seeded in a 6-well plate containing 22 mm round glass coverslips were incubated with the above solutions at 37 °C for 1 and 4 h. After being washed twice with PBS and fixed with 4% formaldehyde, the cell nuclei were stained with Hoechst 33342 for 15 min, and the slides were rinsed three times with PBS. The cellular uptake was visualized by confocal laser scanning microscopy (CLSM) (Olympus, FluoView™ FV3000, Japan) at excitation wavelengths of 405 and 488 nm for Hoechst 33342 and DiO, respectively. On the other hand, TRAMP-C1 cells (2×10^5 cells per well) were incubated with DiO-labeled ZA/PEI@PBCTPNs and ZA/PEI@PCTPNs with and without acid pretreatment, respectively, at a DiO concentration of 0.5 μM at 37 °C for 1 h. After being washed twice with PBS, the treated cells were detached with trypsin-EDTA solution and then dispersed in PBS (0.7 mL). The cellular uptake of various nanoparticles was then analyzed on a flow cytometer (Guava easyCyte HT, Merk Millipore). A minimum of 1×10^4 cells were analyzed from each batch with fluorescence intensity.

2.7. *In vitro* cytotoxicity

To explore the effects of mPEG detachment and surface charge conversion of ZA/PEI@PBCTPNs on their anticancer activity, the ZA/PEI@PBCTPNs were dispersed in PBS of pH 7.4 and 6.5, respectively, at 37 °C for 3 h. Afterward, the ZA/PEI@PBCTPNs were diluted with cell culture medium to the prescribed ZA concentrations. For comparison, the ZA/PEI@PCTPNs were treated by the same way. TRAMP-C1 cells were seeded in a 96-well plate at a density of 1×10^4 cells per well in DMEM (100 μL) containing 10% FBS and 1% penicillin, and incubated at 37 °C for 24 h. The culture medium was then replaced with 100 μL of fresh medium containing free ZA, ZA/PEI@PBCTPNs or ZA/PEI@PCTPNs with and without acid pretreatment at various ZA concentrations, and cells were incubated at 37 °C for an additional 24 h. Afterward, 100 μL MTT (5.0 mg mL^{-1}) was added into each well, followed by incubation at 37 °C for 3 h. After discarding the culture medium, DMSO was added to dissolve the precipitate and the absorbance of the resulting solution at 570 nm was measured using a BioTek 800TS microplate reader. On the other hand, the cytotoxicity of ZA/PEI@PBCTPNs with and without acid pretreatment against HeLa cells and RAW 264.7 cells was evaluated in a similar manner.

2.8. Animals and tumor model

Male C57BL/6J mice (6–8 weeks old), purchased from the National Laboratory Animal Center (Taiwan), were cared for according to the Guidance Suggestions for the Care and Use of Laboratory Animals, approved by the Administrative Committee on Animal Research in the Chung Shan Medical University (Taiwan) (IACUC Approval No: 2514). To establish a xenograft tumor model, a total of 8×10^6 TRAMP-C1 cells were subcutaneously injected into the right thigh of each mouse. The tumor volume (V) was calculated as follows: $V = L \times W^2/2$, where W is the tumor measurement at the widest point and L the tumor dimension at the longest point.

2.9. *In vivo* imaging and biodistribution

In order to observe the *in vivo* biodistribution of ZA/PEI@PBCTPNs and ZA/PEI@PCTPNs by an IVIS imaging system (IVIS Lumina II, Caliper, LifeSciences, MA, USA), a hydrophobic near-infrared (NIR) dye, IR780, was encapsulated into these nanoparticles. The IR780-labeled ZA/PEI@PBCTPNs and ZA/PEI@PCTPNs were prepared by the nanoprecipitation

 This journal is © The Royal Society of Chemistry 2022

Published on 29 April 2022. Downloaded by National Chung Hsing University on 6/16/2022 2:37:46 AM.

method as described in the ESI.† When the tumor volume reached 90–120 mm^3, PBS, free IR780, or various IR780-containing nanoformulations were injected into the mice *via* the tail vein at an IR780 dosage of 1.0 mg kg^{-1}. The fluorescence signals of IR780 (Ex./Em. = 745/810 nm) at 2, 4, 6, 24 and 48 h post-injection were collected by IVIS Lumina II. The treated mice were then sacrificed by CO_2 euthanasia and the major organs harvested for individual organ imaging by IVIS Lumina II.

2.10. *In vivo* tumor growth inhibition

When the tumor volume of the mice approached 90–120 mm^3, the mice were randomly divided into four groups (5 in each group) for different treatments. Before treatment, all the mice were ear-tagged, their initial tumor volumes (V_o) were measured by a caliper, and their average body weights were recorded. All the mice were separately treated by tail-vein injection of either 150 μL PBS, free ZA, ZA/PEI@PBCTPNs or ZA/PEI@PCTPNs at a ZA dosage of 0.8 mg kg^{-1} (half of the MTD of ZA in mice). Each group was treated with a total of two doses at days 0 and 3. The tumor volume and body weight of tumor-bearing mice in the different treatment modalities were monitored every 2 days until the tumor volume increased to beyond 20 times its original volume, at which point the animal was euthanized with an overdose of CO_2. The average growth delay (AGD) and enhancement factor (EF) of each treatment group were attained using a previously reported method.[14] AGD is the difference between the number of days it took the tumor in the treated group to grow to 20 times its initial volume and the time it took the tumor in the untreated control group (injected with PBS only) to reach the same volume. The EF of ZA/PEI@PBCTPNs and ZA/PEI@PCTPNs is the ratio of the AGD of a particular treatment group to the AGD of the treatment group receiving free ZA. The mice tissues, including heart, liver, spleen, lungs and kidneys were excised and fixed with 10% formalin, and then embedded with paraffin wax. The embedded tissues were sectioned into 5 mm for performing hematoxylin and eosin (H&E) staining. The automated TissueFAXS PLUS system was used to acquire section images (TISSUE GNOSTICS, Vienna, Austria).

2.11. Tumor histological evaluation

When the tumor volume of the mice approached 90–120 mm^3, the mice were randomly divided into four groups (3 in each group) for different treatments. All mice were separately treated by tail-vein injection of either 150 μL PBS, free ZA, ZA/PEI@PBCTPNs or ZA/PEI@PCTPNs at a ZA dosage of 0.8 mg kg^{-1}. Each group was treated with a total of two doses at days 0 and 3. 12 days after treatment, mice were euthanized with an overdose of carbon dioxide. The mice tumors were excised, fixed with 10% formalin and then embedded with paraffin wax. The embedded tumors were sectioned into 5 μm and stained with H&E, Ki67 and TUNEL antibodies. Finally, the histological changes, proliferation and apoptosis of tissue cells were observed by the automated TissueFAXS PLUS system (TISSUE GNOSTICS, Vienna, Austria).

2.12. Statistical analysis

Data were reported as mean ± SD. The differences among groups were determined using one-way ANOVA analysis; n.s. = statistically insignificant, (*) $P < 0.05$, (**) $P < 0.005$ and (***) $P < 0.001$.

3. Results and discussion

3.1. Synthesis and characterization of mPEG-*b*-C18 and mPEG-C18 adducts

The mPEG-*b*-C18 employed in this study was obtained by the coupling of mPEG-CHO with 1-octadecylamine upon Schiff base reaction. As presented in the ^{1}H-NMR spectrum of mPEG–CHO (Fig. 1a), the appearance of feature proton signals of the benzene ring at δ 8.1 and 8.3 ppm, and of the aldehyde group at δ 10.1 ppm confirmed the successful conjugation of mPEG-OH and 4-formylbenzoic acid. The coupling efficiency was estimated to be *ca.* 97% based on the signal integral ratio of the methoxy protons (δ 3.4 ppm) and aldehyde protons (δ 10.1 ppm) of mPEG-CHO. The ^{1}H-NMR spectrum of mPEG-*b*-C18 (Fig. 1b) showed that the proton signals of aliphatic alkyl moieties from octadecane and the resulting imine groups appeared at δ 0.8–1.8 ppm and δ 8.4 ppm, respectively, strongly demonstrating the effective conjugation of mPEG–CHO and 1-octadecylamine. The conjugation efficiency was attained to be *ca.* 95% according to the signal integral ratio of the methyl and imine protons of mPEG-*b*-C18. For comparison, through the esterification of mPEG-OH with stearic acid, the mPEG-C18 adducts lacking an acid-labile benzoic imine bond were obtained and then characterized by ^{1}H-NMR (Fig. 1c). Based on the integral ratio of the signals from the tail methyl protons (δ 0.82 ppm) of stearic acid and methoxy protons (δ 3.4 ppm) of mPEG, the coupling efficiency was attained to be *ca.* 95%. Importantly, as presented in the ^{1}H-NMR spectrum of mPEG-*b*-C18 adducts exposed to an acidic environment (pH 6.5 for 3 h) (Fig. 1d), the disappearance of proton signals of the imine group at δ 8.4 ppm and the appearance of the proton signals of

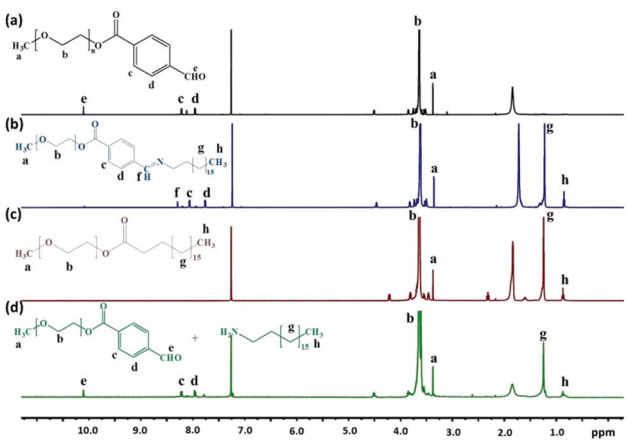

Fig. 1 ^{1}H-NMR spectra of (a) mPEG-CHO, (b) mPEG-*b*-C18, (c) mPEG-C18 and (d) acid-pretreated mPEG-*b*-C18 in $CDCl_3$.

Published on 29 April 2022. Downloaded by National Chung Hsing University on 6/16/2022 2:37:46 AM.

the aldehyde group at δ 10.1 ppm clearly illustrate the acid-elicited cleavage of the benzoic imine bond of mPEG-*b*-C18.

3.2. Preparation and characterization of ZA/PEI-encapsulated hybrid polymeric nanoparticles

In this work, the ZA-carrying nanoparticles coated with amphiphilic TPGS and either mPEG-*b*-C18 or mPEG-C18 were attained using a one-pot nanoprecipitation method. As revealed in Table 1, compared to the ZA@PBCTPNs with quite low DLE (*ca.* 13.3%), the ZA/PEI@PBCTPNs (N/P ratio = 4.5) exhibited higher DLE (*ca.* 46.3%). This is well consistent with our previous study in which the ionic pairings of positively-charged PEI segments (M.W. = 10 kDa) with negatively-charged ZA molecules effectively promoted encapsulation of ZA into the PLGA-rich core of hybrid nanoparticles composed of PLGA-*b*-PEG and TPGS segments.[19] Considering the lower cytotoxicity of short PEI segments compared to that of long PEI segments as reported elsewhere,[31,32] the short PEI segments (1.8 kDa) were utilized in this study. Note that when the N/P ratio of ZA/PEI complexes in the feed was adjusted from 4.5 to 9.0, the ZA loading efficiency of ZA/PEI@PBCTPNs was remarkably elevated from 46.3 to 83.5%. The resulting ZA/PEI@PBCTPNs (9.0) exhibited prominent drug loading capacity (*ca.* 12.3 wt%). Therefore, for maintaining adequate ZA loading content, the N/P ratio of 9.0 for ZA/PEI complexes was employed in the preparation of ZA/PEI@PBCTPNs and ZA/PEI@PCTPNs. As presented in Table 1 and Fig. 2a, the mean hydrodynamic diameter (D_h) of the ZA/PEI@PBCTPNs in PBS was *ca.* 132.9 nm, being somewhat larger than that (*ca.* 125.3 nm) of ZA/PEI@PCTPNs. This could be ascribed to the extensive π–π stacking and hydrophobic interaction of benzene ring-containing mPEG-*b*-C18 adducts with TPGS tending to form a thick coating layer on particle surfaces. Interestingly, distinct from the well suspension of ZA/PEI@PBCTPNs in PBS, serious aggregation and precipitation of ZA/PEI@TPNs (with TPGS alone) and ZA/PEI@PBCPNs (with mPEG-*b*-C18 alone) in PBS were observed (Fig. S1, ESI†). This implies that the hydrophobic co-anchor effect of amphiphilic mPEG-*b*-C18 and TPGS on the surfaces of hybrid nanoparticles plays a crucial role in stabilizing the colloidal structure, although the alignment of these molecules on the molecular level is currently not clear. For ZA/PEI@PBCTPNs and ZA/PEI@PCTPNs, a highly linear relationship between the relaxation frequency (Γ) and the square of the scattering vector (q^2) in the variable angle DLS data was attained (Fig. 2b and c), indicating the nearly spherical shape of these nanoparticles in pH 7.4 PBS.[19] Also, the well-dispersed spherical morphology of ZA/PEI@PBCTPNs and ZA/PEI@PCTPNs was observed in their TEM images (Fig. 2d and Fig. S2, ESI†).

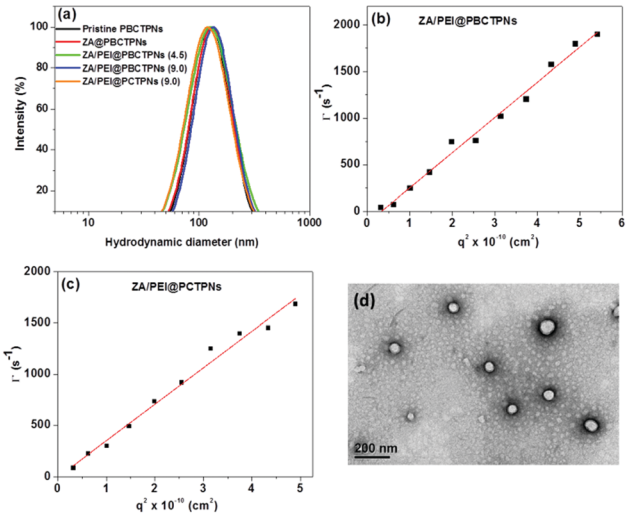

Fig. 2 (a) DLS size distribution profiles of various nanoparticles in pH 7.4 PBS. Angle-dependent correlation of Γ *versus* q^2 of (b) ZA/PEI@PBCTPNs and (c) ZA/PEI@PCTPNs in pH 7.4 PBS. (d) TEM images of ZA/PEI@PBCTPNs.

The colloidal stability of ZA-carrying hybrid polymeric nanoparticles in PBS containing 10% FBS was also assessed by DLS measurements. Notably, for the ZA/PEI@PBCTPNs and ZA/PEI@PCTPNs, no remarkable variation in particle size and size distribution was observed within 24 h (Fig. 3a and b), indicating that the outer hydrophilic PEG segments of hybrid polymeric nanoparticles could prevent interparticle aggregation under serum-containing conditions. Also, the ZA/PEI@PBCTPNs and ZA/PEI@PCTPNs suffered from large-volume dilution with pH 7.4 PBS maintained with a virtually unvaried particle size (Fig. 3c and d). In view of these findings, it is presumed that the robust ZA/PEI-encapsulated hybrid nanoparticles can well hold colloidal integrity during blood circulation after intravenous injection to avoid burst leakage of ZA and interparticle aggregation.

3.3. Acidity-triggered mPEG detachment and surface charge conversion

As shown in Fig. 4a, in the absence of PEI segments, the resulting ZA@PBCTPNs exhibited a negative zeta potential value (−9.0 mV) at pH 7.4, indicating that most of the bisphosphonate-bearing ZA molecules were apt to attach on the surfaces of hybrid nanoparticles, thereby increasing negative charges on colloidal surfaces. By contrast, the zeta potential

Table 1 DLS data, drug loading efficiency and content of ZA-loaded nanoparticles

Sample	D_h (nm)	PDI	DLE (%)	DLC (wt%)
PEI@PBCTPNs	128.9 ± 1.3	0.218 ± 0.037	—	—
ZA@PBCTPNs	129.9 ± 2.3	0.187 ± 0.001	13.3 ± 6.2	4.1 ± 1.8
ZA/PEI@PBCTPNs (4.5)	126.6 ± 6.2	0.242 ± 0.004	46.3 ± 8.9	9.2 ± 1.6
ZA/PEI@PBCTPNs (9.0)	132.9 ± 7.4	0.220 ± 0.043	83.5 ± 7.0	12.3 ± 0.9
ZA/PEI@PCTPNs (9.0)	125.3 ± 7.5	0.200 ± 0.017	58.1 ± 9.1	7.8 ± 1.4

 This journal is © The Royal Society of Chemistry 2022

Published on 29 April 2022. Downloaded by National Chung Hsing University on 6/16/2022 2:37:46 AM.

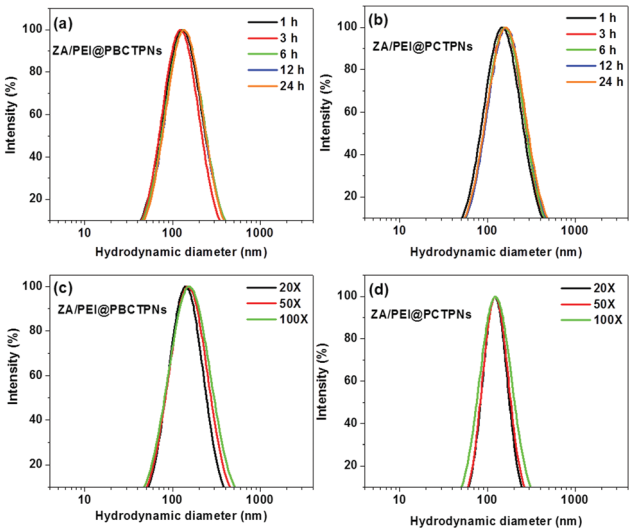

Fig. 3 DLS size distribution profiles of (a) ZA/PEI@PBCTPNs and (b) ZA/PEI@PCTPNs dispersed in 10% FBS-containing PBS at different time intervals, and (c) ZA/PEI@PBCTPNs and (d) ZA/PEI@PCTPNs upon pH 7.4 PBS dilution.

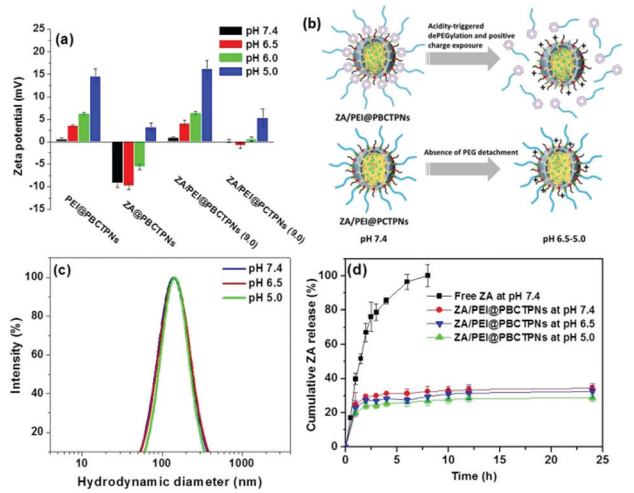

Fig. 4 (a) Zeta potential of various hybrid nanoparticles in aqueous solutions of different pH values. (b) Schematic illustration of the structural transition of ZA/PEI@PBCTPNs and ZA/PEI@PCTPNs in response to pH reduction. (c) DLS size distribution profiles of ZA/PEI@PBCTPNs in aqueous solutions of different pH. (d) Cumulative ZA release profiles of ZA/PEI@PBCTPNs at pH 7.4, 6.5 and 5.0 at 37 °C by the dialysis method. Diffusion of free ZA molecules across the dialysis tube is included for comparison.

values of ZA/PEI@PBCTPNs and ZA/PEI@PCTPNs were determined to be nearly zero, suggesting that the formation of ionic ZA/PEI complexes facilitated the encapsulation of ZA into a hydrophobic PLGA-constituted core. More importantly, with the solution pH being adjusted from pH 7.4 to 5.0, significant conversions in zeta potentials of ZA/PEI@PBCTPNs and PEI@PBCTPNs from virtually neutral to appreciably positive values were attained. As expected, through the acidity-elicited cleavage of benzoic imine linkers in mPEG-*b*-C18 adducts, the mPEG segments were detached from the above hybrid nanoparticles, thereby exposing positive charges of protonated PEI segments on the nanoparticle surfaces to elevate the zeta potential (Fig. 4b). In contrast, only a slight change in the zeta potential of ZA/PEI@PCTPNs was observed with the pH reduction (Fig. 4a). This is because the outer mPEG segments were incapable of separating from ZA/PEI@PCTPNs due to the absence of acid-labile linkages in mPEG-C18 adducts largely shielding the positive charges of protonated PEI segments on the nanoparticle surfaces (Fig. 4b). Such a considerable change in zeta potential of varied PEGylated nanoparticles in response to acidity-triggered PEG detachment has also been reported elsewhere.[33,34] Notably, when exposed to a weak acidic environment (pH 6.5 and 6.0) close to the pH_e where dePEGylation occurred, compared to the ZA@PBCTPNs with negatively charged surfaces, the ZA/PEI@PBCTPNs exhibited somewhat positively charged surfaces (Fig. 4a). This evidently demonstrates that the incorporation of PEI segments into hybrid nanoparticles not only assists the encapsulation of massive ZA molecules into nanoparticles but also provides additional positive charges on the nanoparticle surfaces. Furthermore, no significant variation in the particle size of ZA/PEI@PBCTPNs was attained with pH reduction from 7.4 to 5.0 (Fig. 4c), illustrating that these therapeutic nanoparticles after mPEG detachment still retained a highly stable colloidal structure without dissociation or inter-particle aggregation. It is worth mentioning that the ZA/PEI@PBCTPNs exhibit positively charged surfaces and a robust architecture when exposed to the weak acidic milieu (pH 6.5), an essential prerequisite for effective intracellular ZA delivery. Based on the results, it was assumed that the uptake of ZA/PEI@PBCTPNs within an acidic tumor extracellular matrix by cancer cells and TAMs could be promoted upon the acid-activated mPEG detachment and exposure of some positive charges on colloidal surfaces, thus enhancing the ZA-mediated anticancer potency.

3.4. *In vitro* ZA release

Different from rapid diffusion of free ZA molecules across the dialysis tube (over 75% within 3 h) in pH 7.4 PBS, only less than 30% of ZA was liberated from ZA/PEI@PBCTPNs (Fig. 4d). Also, a significantly reduced ZA release (below 35% over 3 h) of ZA/PEI@PCTPNs under the same condition was attained (data not shown). These results strongly suggest that the encapsulation of ZA/PEI complexes into hydrophobic PLGA-based cores could considerably prevent burst ZA leakage from hybrid nanoparticles. Similar findings regarding the largely declined premature release of ZA from ZA/Ca complex-encapsulated PLGA nanoparticles were also reported by Cui's group.[18] For ZA/PEI@PBCTPNs, this considerable reduction in premature ZA leakage is expected to be beneficial for sufficient accumulation of ZA within the extraskeletal tumors upon the EPR effect. Furthermore, ZA release of ZA/PEI@PBCTPNs was not remarkably promoted in response to pH decrease from 7.4 to 6.5 and 5.0, signifying that the acid-activated mPEG detachment from nanoparticle surfaces cannot accelerate ZA liberation. As

Published on 29 April 2022. Downloaded by National Chung Hsing University on 6/16/2022 2:37:46 AM.

presented in some previous studies,[35,36] the release of therapeutic reagents encapsulated within PLGA-rich nanoparticles generally depended on the diffusion of molecules across the polymer matrix upon the acid/enzyme-mediated gradual hydrolysis and/or erosion of PLGA segments within the acidic endosomes and lysosomes.

3.5. *In vitro* cellular uptake and cytotoxicity

To evaluate the cellular uptake of ZA-carrying hybrid nanoparticles by TRAMP-C1 cells, the hydrophobic fluorescent dye, DiO, was incorporated into these nanoparticles for fluorescence imaging. As revealed in the CLSM images (Fig. 5a), after 1 h and 4 h cell incubation, the DiO fluorescence signals (green) of DiO-labeled ZA/PEI@PBCTPNs with acid pretreatment were observed largely in the cytoplasm of TRAMP-C1 cells, whereas quite weak DiO fluorescence signals of the counterparts without acid pretreatment were found intracellularly. Also, the quantified DiO fluorescence intensity of TRAMP-C1 cells receiving acid-pretreated DiO-labeled ZA/PEI@PBCTPNs for 1 and 4 h, respectively, was prominently 4.5 and 4.6-fold higher than that of cells treated with the counterparts with the lack of acid pretreatment (Fig. 5b). This increase in DiO fluorescence intensity of TRAMP-C1 cells incubated with the acid-pretreated ZA/PEI@PBCTPNs for 1 h was also confirmed by flow cytometric histograms (Fig. 5c). Note that TRAMP-C1 cells exposed to DiO-labeled ZA/PEI@PCTPNs with and without acid pretreatment displayed very low DiO fluorescence intensity (Fig. 5a and b). The above results strongly verify that the ZA/PEI@PBCTPNs undergoing acidity-elicited mPEG detachment and surface positive charge exposure can effectively enhance cellular uptake upon the promoted affinity with the negatively-charged cell membranes (Fig. 5d). This boosted cellular uptake of functionalized nanoparticles by PEG detachment and surface charge conversion has been reported elsewhere.[34,37] By contrast, the cellular internalization of ZA/PEI@PCTPNs was largely restricted due to the lack of dePEGylation (Fig. 5d).

In view of the promoted cellular uptake of acid-pretreated ZA/PEI@PBCTPNs, their anticancer potency on TRAMP-C1 cells was further evaluated. As an important control, TRAMP-C1 cells incubated with ZA-free PEI@PBCTPNs (12–196 μg mL^{-1}) for 48 h maintained relatively high viability beyond 80%, being indicative of the low toxicity of these nanocarriers toward cancer cells (Fig. 6a). When TRAMP-C1 cells were incubated with free ZA molecules in the drug concentration range 6.25–100 μM, the cell viability was appreciably reduced in a ZA concentration-dependent manner (Fig. 6b), illustrating the anticancer activity of ZA. Furthermore, free ZA molecules receiving acid pretreatment or not showed similar cytotoxicity toward TRAMP-C1 cells. Note that the ZA/PEI@PBCTPNs after acid pretreatment displayed considerably enhanced cytotoxicity

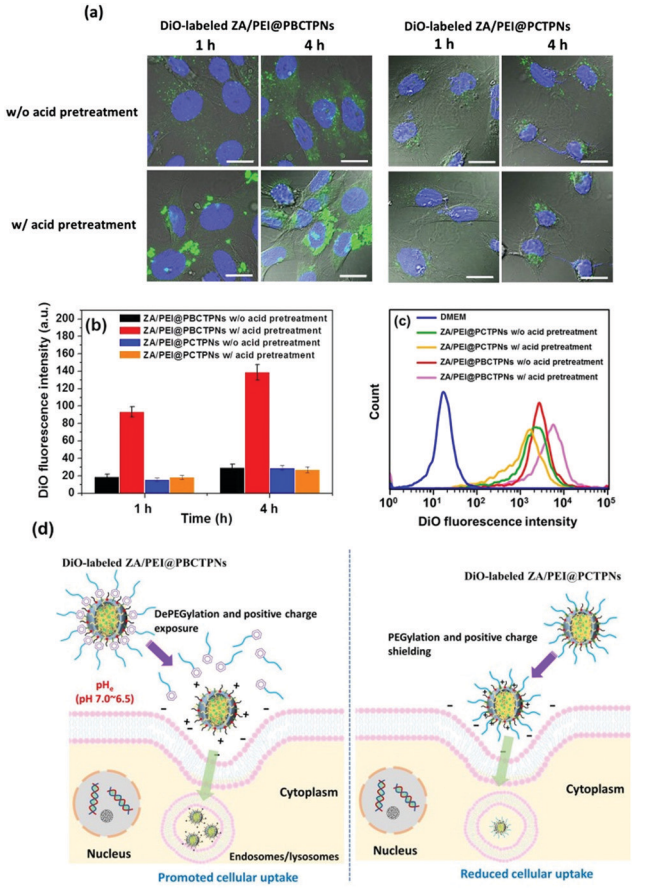

Fig. 5 (a) CLSM images and (b) quantified DiO fluorescence intensity of TRAMP-C1 cells incubated with DiO-labeled ZA/PEI@PBCTPNs and ZA/PEI@PCTPNs with and without acid pretreatment at 37 °C for 1 and 4 h, respectively. Nuclei were stained with Hoechst. Scale bars are 15 μm. (c) Flow cytometric histograms of TRAMP-C1 cells exposed to DiO-labeled ZA/PEI@PBCTPNs and ZA/PEI@PCTPNs with and without acid pretreatment for 1 h (DiO concentration = 0.5 μM). (d) Schematic illustration of the cellular uptake of acid-pretreated DiO-labeled ZA/PEI@PBCTPNs and ZA/PEI@PCTPNs by cancer cells.

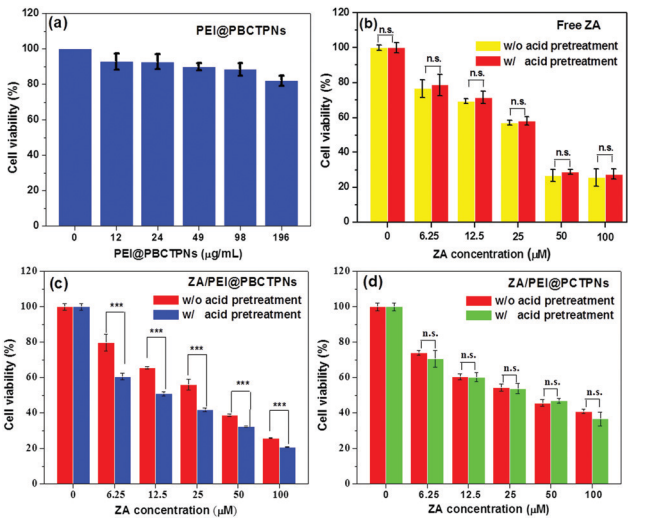

Fig. 6 Cell viability of TRAMP-C1 cells incubated with (a) PEI@PBCTPNs at 37 °C for 48 h and (b) free ZA molecules with and without acid pretreatment at 37 °C for 24 h. Cell viability of TRAMP-C1 cells treated with (c) ZA/PEI@PBCTPNs and (d) ZA/PEI@PCTPNs with and without acid pretreatment at 37 °C for 24 h. n.s. = statistically insignificant, $*P < 0.05$, $**P < 0.005$, $***P < 0.001$.

This journal is © The Royal Society of Chemistry 2022

Published on 29 April 2022. Downloaded by National Chung Hsing University on 6/16/2022 2:37:46 AM.

against TRAMP-C1 cells in comparison with the counterparts without acid pretreatment (Fig. 6c). The attained drug doses required for 50% cellular growth inhibition (IC_{50}) of ZA/PEI@PBCTPNs with and without acid pretreatment are *ca.* 13.2 and 29.4 μM, respectively. Similar findings were also obtained with another cell model, human cervical HeLa cancer cells (Fig. S3, ESI†). By contrast, no significant difference in cytotoxicity effect of ZA/PEI@PCTPNs with and without acid pretreatment on TRAMP-C1 and HeLa cells was observed (Fig. 6d and Fig. S3, ESI†). More importantly, after acid pretreatment, the ZA/PEI@PBCTPNs exhibited a 3-fold lower IC_{50} (13.2 μM) on TRAMP-C1 cells compared to ZA/PEI@PCTPNs (IC_{50} = 41.1 μM), illustrating that the acidity-elicited dePEGylation and surface positive charge exposure of the former profoundly boosted their cellular uptake and anticancer potency, while the non-detachable mPEG coating of the latter considerably lowered their cellular internalization and anticancer efficacy.

On the other hand, in view of several studies revealing the high correlation of TAMs to tumor progression and metastasis,[38,39] TAMs have emerged as potential targets for cancer treatment. Considering that ZA has been demonstrated to be a potent regent for killing of macrophages,[11,12,18,40] to preliminarily evaluate the feasibility of ZA/PEI@PBCTPNs as an antitumor reagent, their cellular uptake and cytotoxicity on the murine macrophages RAW 264.7 were further explored. As presented in Fig. 7a, the DiO fluorescence signals of RAW 264.7 cells receiving DiO-labeled ZA/PEI@PBCTPNs with acid pretreatment for 4 h were remarkably enhanced as compared to those of the cells treated with the counterparts without acid pretreatment. By contrast, RAW 264.7 cells exposed to DiO-labeled ZA/PEI@PCTPNs with and without acid pretreatment revealed minor DiO fluorescence intensity. Similar results were also observed in Fig. S4 (ESI†). Undoubtedly, the affinity of DiO-labeled ZA/PEI@PBCTPNs for RAW 264.7 cells was considerably increased by the acidity-triggered dePEGlation and surface charge conversion, thus promoting their internalization by macrophages RAW 264.7. In the presence of non-detachable mPEG segments, the internalization of ZA/PEI@PCTPNs by RAW 264.7 cells was significantly hindered.

Compared to quite high viability of RAW 264.7 cells incubated with PEI@PBCTPNs (Fig. S5, ESI†), the viability of RAW 264.7 cells treated with either free ZA or ZA/PEI@PBCTPNs was appreciably reduced in a ZA concentration-dependent manner (Fig. 7b and c), signifying the effective cytotoxicity of ZA against RAW 264.7 cells. Notably, the ZA/PEI@PBCTPNs after acid pretreatment exhibited considerably superior capability of inhibiting proliferation of RAW 264.7 cells compared to the counterparts without acid pretreatment (Fig. 7c). The IC_{50} values of ZA/PEI@PBCTPNs with and without acid pretreatment on RAW 264.7 cells were obtained to be *ca.* 8.0 and 14.3 μM, respectively. Based on the above findings, this enhanced cytotoxicity of the acid-pretreated ZA/PEI@PBCTPNs on the macrophages could be attributed to their promoted cellular uptake provoked by mPEG detachment and surface positive charge exposure. In view of the increased cellular uptake and cytotoxicity of ZA/PEI@PBCTPNs on cancer cells and macrophages in response to a weak acidic environment, it was anticipated that the accumulation of ZA/PEI@PBCTPNs within an acidic tumor microenvironment could be appreciably increased to boost the ZA-associated antitumor effect.

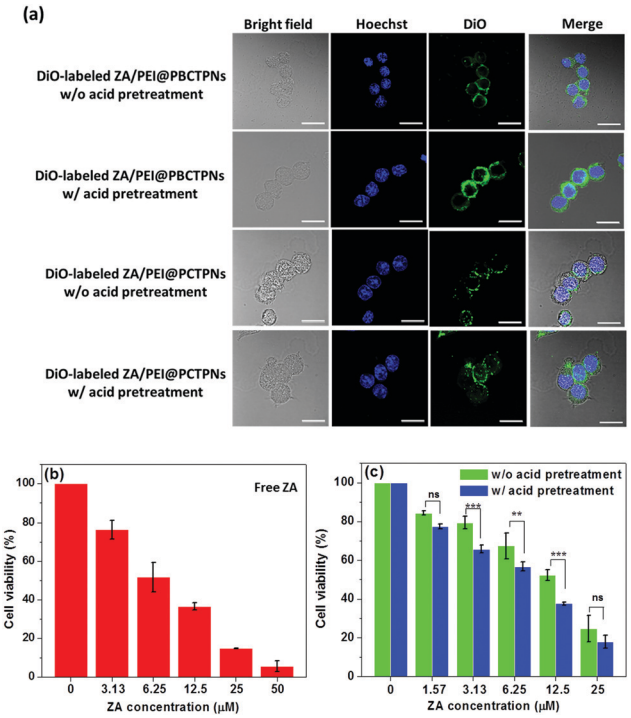

Fig. 7 (a) CLSM images of RAW 264.7 cells incubated with DiO-labeled ZA/PEI@PBCTPNs and ZA/PEI@PCTPNs with and without acid pretreatment at 37 °C for 4 h, respectively. Nuclei were stained with Hoechst. The scale bars are 20 μm. Cell viability of RAW 264.7 cells incubated with either (b) free ZA or (c) ZA/PEI@PBCTPNs with and without acid pretreatment at 37 °C for 48 h. n.s. = statistically insignificant, $*P < 0.05$, $**P < 0.005$, $***P < 0.001$.

3.6. *In vivo* biodistribution

In order to explore the *in vivo* tumor accumulation and biodistribution of ZA/PEI@PBCTPNs by an IVIS imaging system, a hydrophobic NIR dye, IR780, was encapsulated into these nanoparticles. The IR780-labeled ZA/PEI@PCTPNs which lacked dePEGylation capability were employed as the control. Note that for the IR780-labeled ZA/PEI@PBCTPNs and ZA/PEI@PCTPNs separately dispersed in PBS with and without 10% FBS, no considerable change in particle size was observed within 24 h (Fig. S6, ESI†), indicating that the encapsulation of IR780 molecules did not impair the colloidal stability of these nanoparticles. After intravenous injections with free IR780 or various IR780-labeled nanoparticles, the nanoparticle accumulation in tumor sites of TRAMP-C1 tumor-bearing mice was monitored by IR780 NIR fluorescence imaging. As shown in Fig. 8a and b, over the time period of post-injection, the IR780-labeled ZA/PEI@PBCTPN and ZA/PEI@PCTPN groups exhibited stronger fluorescence signals in the tumor regions as compared to the free IR780 group. This suggests that the tumor

Published on 29 April 2022. Downloaded by National Chung Hsing University on 6/16/2022 2:37:46 AM.

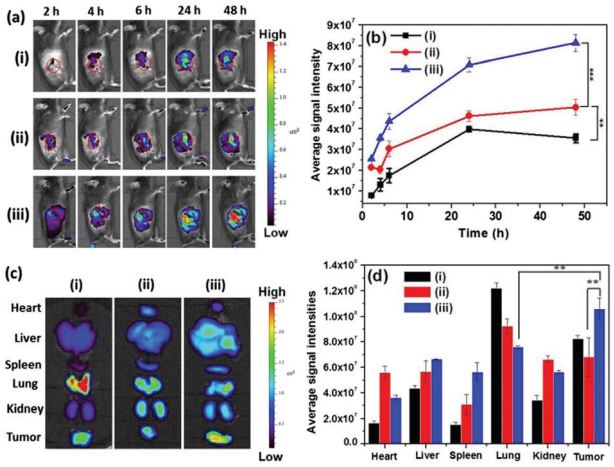

Fig. 8 (a) *In vivo* NIR images and (b) average IR780 fluorescence intensities of TRAMP-C1 tumor-bearing mice receiving intravenous injection of (i) free IR780, (ii) IR780-labeled ZA/PEI@PCTPNs and (iii) IR780-labeled ZA/PEI@PBCTPNs, respectively, obtained by IVIS (n = 3 per group). Tumor sites are labeled with red circles. (c) NIR fluorescence images and (d) average IR780 fluorescence intensities of the isolated major organs and tumors from TRAMP-C1 tumor-bearing mice at 48 h post-injection with (i) free IR780, (ii) IR780-labeled ZA/PEI@PCTPNs and (iii) IR780-labeled ZA/PEI@PBCTPNs, respectively. n.s. = statistically insignificant, $*P < 0.05$, $**P < 0.005$, $***P < 0.001$.

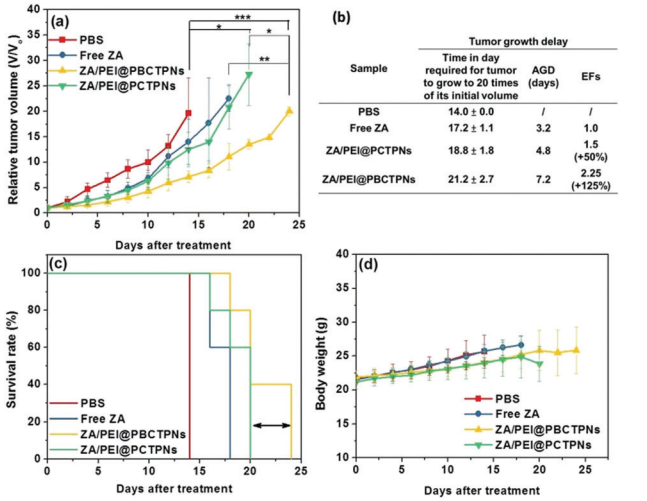

Fig. 9 (a) Tumor growth inhibition profiles of TRAMP-C1 tumor-bearing mice intravenously injected with PBS, free ZA, ZA/PEI@PBCTPNs or ZA/PEI@PCTPNs (n = 5 per group). (b) *In vivo* antitumor efficacies of free ZA and ZA-carrying nanoparticles. (c) Survival rate and (d) body weight of TRAMP-C1 tumor-bearing mice receiving PBS, free ZA, ZA/PEI@PBCTPNs or ZA/PEI@PCTPNs. n.s. = statistically insignificant, $*P < 0.05$, $**P < 0.005$, $***P < 0.001$.

accumulation of IR780-labeled hybrid nanoparticles was enhanced by the EPR effect, thus preventing IR780 molecules from degradation and body clearance. Note that the IR780 fluorescence intensity at tumor sites of the IR780-labeled ZA/PEI@PBCTPN group was markedly higher than that of the IR780-labeled ZA/PEI@PCTPN group over the time course. Also, as shown in the *ex vivo* NIR fluorescence images and intensities (Fig. 8c and d), the tumors receiving IR780-labeled ZA/PEI@PBCTPNs at 48 h post-injection exhibited higher fluorescence intensities than those treated with free IR780 or IR780-labeled ZA/PEI@PCTPNs. Also, for the IR780-labeled ZA/PEI@PBCTPNs group, the *ex vivo* IR780 fluorescence intensity of the tumor was appreciably higher than that in the liver and lung. Based on the above findings, it was demonstrated that the deposition of ZA/PEI@PBCTPNs within tumor sites was remarkably promoted by the increased cellular uptake due to tumor acidity-elicited PEG detachment and surface positive charge exposure. This enhanced tumor accumulation of ZA/PEI@PBCTPNs would be favorable for the treatment of extra-skeletal solid tumors by ZA-mediated cytotoxicity. For IR780-labeled ZA/PEI@PCTPNs, due to the lack of PEG detachment, an accumulation in tumors comparable to the liver, lungs and kidneys was attained.

3.7. *In vivo* antitumor potency

The tumor size and body weight of TRAMP-C1 tumor-bearing mice were monitored post intravenous injection of various ZA-carrying nanoparticles to evaluate the antitumor activity. In this work, PBS was adopted as a control, free ZA, ZA/PEI@PBCTPNs and ZA/PEI@PCTPNs were applied at a ZA dosage of 0.8 mg kg^{-1}, and the doses were given by tail vein at days 0 and 3. The tumor volumes (V) were normalized against their initial volume (V_o) to attain the relative tumor volume (V/V_o). As presented in the tumor-growth delay data (Fig. 9a and b), the administration of free ZA and ZA/PEI@PCTPNs delayed the growth of TRAMP-C1 tumors by an average of 3.2 and 4.8 days, respectively, compared with the control group. Notably, the treatment of ZA/PEI@PBCTPNs further delayed the growth of TRAMP-C1 tumors by 7.2 days relative to the control group. Quantitative tumor growth delay data illustrated that the ZA/PEI@PBCTPNs considerably enhanced the antitumor activity of ZA by 125% in TRAMP-C1 tumors in comparison with the ZA/PEI@PCTPNs (*ca.* 50%) (Fig. 9b). Importantly, the survival rate of the tumor-bearing mice receiving ZA/PEI@PBCTPNs was appreciably elevated compared to other treated groups (Fig. 9c). Based on these findings, it can be concluded that the ZA/PEI@PBCTPNs undergoing tumor acidity-triggered dePEGylation and surface charge conversion could effectively promote the tumor uptake of ZA, thereby hindering TRAMP-C1 tumor growth and prolonging survival of the treated mice. By contrast, due to poor cellular uptake in the absence of dePEGylation, the ZA/PEI@PCTPNs were incapable of inhibiting tumor growth in an effective manner. On the other hand, no significant variation in the body weights of the treated mice in all groups was obtained, signifying that the formulations utilized in this study did not provoke serious acute toxicity (Fig. 9d). Also, no apparent abnormality was attained in the major organs of mice treated with all ZA-carrying nanoparticles (Fig. S7, ESI†). These results strongly suggest that the ZA/PEI@PBCTPNs developed herein not only have no adverse effect on normal tissues, but also show a satisfactory anticancer efficacy.

This journal is © The Royal Society of Chemistry 2022

Published on 29 April 2022. Downloaded by National Chung Hsing University on 6/16/2022 2:37:46 AM.

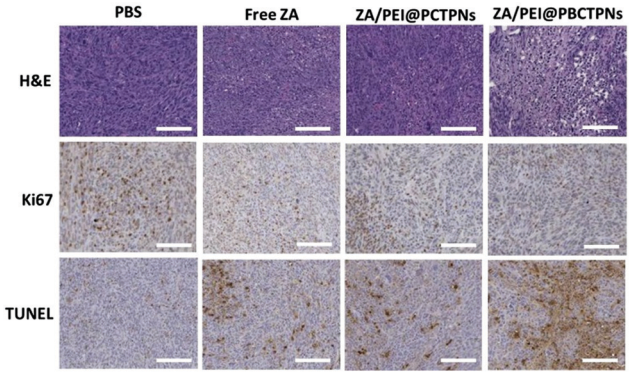

Fig. 10 H&E, Ki67 and TUNEL protein analysis of tumor sections from the TRAMP-C1 tumor-bearing mice receiving PBS, free ZA, ZA/PEI@PBCTPNs or ZA/PEI@PCTPNs. Scale bars are 100 μm.

3.8. Tumor histological insight

Further tumor histological studies were executed to gain insight into the antitumor effect of the small-molecule ZA and ZA-containing hybrid nanoparticles. Representative TRAMP-C1 xenograft tumors were harvested at 12 days after chemotherapy to explore the therapeutic effects of various treatments. As shown in Fig. 10, in contrast to the normal tumor growth status of the PBS group, the treated groups displayed various degrees of tissue necrosis, nuclear shrinkage and debris. Notably, the ZA/PEI@PBCTPNs group exhibited the highest degree of necrosis and nuclear shrinkage, revealing the most powerful antitumor efficacy. Also, this group displayed lower expression of Ki67, a marker of cell proliferation, compared to other groups, and the largest apoptotic regions stained by TUNEL. The histological studies further confirmed that the tumor acidity-responsive ZA/PEI@PBCTPNs boosted ZA-mediated antitumor potency upon the promoted tumor accumulation and cellular uptake.

4. Conclusions

To facilitate the practical application of ZA in the treatment of extraskeletal solid tumors by improving intracellular ZA delivery, through co-assembly of hydrophobic PLGA, amphiphilic TPGS and mPEG-*b*-C18 to encapsulate ionic ZA/PEI complexes, versatile ZA/PEI@PBCTPNs with acidity-triggered detachable PEG shells and switchable surface charges were developed. The attained ZA/PEI@PBCTPNs with high ZA payloads not only maintained a well-dispersed colloidal structure in serum-containing aqueous solutions but also prominently decreased burst ZA leakage. The *in vitro* cellular uptake and cytotoxicity studies revealed that the uptake of ZA/PEI@PBCTPNs by TRAMP-C1 cells as well as macrophage-like RAW 264.7 cells was considerably promoted upon acidity-triggered mPEG detachment and surface positive charge exposure, thus remarkably enhancing ZA cytotoxicity. Importantly, compared to PEG non-detachable ZA/PEI@PCTPNs, the ZA/PEI@PBCTPNs effectively accumulated within tumor sites and delayed tumor growth *in vivo*, thus increasing the survival rate of treated mice. These results strongly demonstrate that the designed tumor acidity-responsive ZA/PEI@PBCTPNs have significant potential for achieving clinical applications of ZA molecules in the treatment of extraskeletal tumors.

Conflicts of interest

There are no conflicts to declare.

Acknowledgements

This work is supported by the Ministry of Science and Technology (MOST 108-2221-E-005-024-MY2, MOST 110-2628-E-005-001, MOST110-2731-M-005-001), National Chung Hsing University and Chung Shan Medical University (NCHU-CSMU 11003), Taiwan.

References

1 G. Li, L. Zhang, L. Wang, G. Yuan, K. Dai, J. Pei and Y. Hao, *Acta Biomater.*, 2018, **65**, 486–500.
2 L. Wang, D. Fang, J. Xu and R. Luo, *BMC Cancer*, 2020, **20**, 1059.
3 W. Sun, K. Ge, Y. Jin, Y. Han, H. Zhang, G. Zhou, X. Yang, D. Liu, H. Liu, X. J. Liang and J. Zhang, *ACS Nano*, 2019, **13**, 7556–7567.
4 H. Geng, M. Zhou, B. Li, L. Liu, X. Yang, Y. Wen, H. Yu, H. Wang, J. Chen and L. Chen, *Chem. Eng. J.*, 2021, **417**, 128103.
5 J. Zekri, M. Mansour and S. M. Karim, *J. Bone Oncol.*, 2014, **3**, 25–35.
6 X. Li, Y. W. Nagui and Z. Cui, *Int. J. Pharm.*, 2017, **526**, 69–76.
7 K. McKeage and G. L. Plosker, *Pharmacoeconomics*, 2008, **26**, 251–268.
8 H. Almubarak, A. Jones, R. Chaisuparat, M. Zhang, T. F. Meiller and M. A. Scheper, *J. Carcinog.*, 2011, **10**, 2.
9 C. Borghese, N. Casagrande, E. Pivetta, A. Colombatti, M. Boccellino, E. Amler, N. Normanno, M. Caraglia, G. D. Rosa and D. Aldinucci, *Oncotarget*, 2017, **8**, 42926–42938.
10 J. R. Ross, Y. Saunders, P. M. Edmonds, S. Patel, K. E. Broadley and S. R. Johnston, *BMJ*, 2003, **327**, 469.
11 X. Zang, X. Zhang, H. Hu, M. Qiao, X. Zhao, Y. Deng and D. Chen, *Mol. Pharmaceutics*, 2019, **16**, 2249–2258.
12 X. Tang, D. Sui, M. Liu, H. Zhang, M. Liu, S. Wang, D. Zhao, W. Sun, M. Liu, X. Luo, X. Lai, X. Liu, Y. Deng and Y. Song, *Int. J. Pharm.*, 2020, **590**, 119929.
13 M. McClung, *Arq. Bras. Endocrinol. Metabol.*, 2006, **50**, 735–744.
14 K. M. Au, A. Satterlee, Y. Min, X. Tian, Y. S. Kim, J. M. Caster, L. Zhang, T. Zhang, L. Huang and A. Z. Wang, *Biomaterials*, 2016, **82**, 178–193.
15 H. Shmeeda, Y. Amitay, D. Tzemach, J. Gorin and A. Gabizon, *J. Controlled Release*, 2013, **167**, 265–275.
16 M. Marra, G. Salzano, C. Leonetti, M. Porru, R. Franco, S. Zappavigna, G. Liguori, G. Botti, P. Chieffi, M. Lamberti,

Published on 29 April 2022. Downloaded by National Chung Hsing University on 6/16/2022 2:37:46 AM.

G. Vitale, A. Abbruzzese, M. I. La Rotonda, G. De Rosa and M. Caraglia, *Biotechnol. Adv.*, 2012, **30**, 302–319.
17 Q. Guo, X. He, C. Li, Y. He, Y. Peng, Y. Zhang, Y. Lu, X. Chen, Y. Zhang, Q. Chen, T. Sun and C. Jiang, *Adv. Sci.*, 2019, **6**, 1901430.
18 X. Li, S. A. Valdes, R. F. Alzhrani, S. Hufnagel, S. D. Hursting and Z. Cui, *ACS Appl. Mater. Interfaces*, 2019, **11**, 7311–7319.
19 M. C. Xiao, Y. H. Chou, Y. N. Hung, S. H. Hu and W. H. Chiang, *Mater. Sci. Eng., C*, 2020, **116**, 111277.
20 J. Liu, D. S. Karaman, J. Zhang, J. M. Rosenholm, X. Guo and K. Cai, *J. Mater. Chem. B*, 2017, **5**, 8289–8298.
21 D. K. Khajuria, R. Razdan and D. R. Mahapatra, *Eur. J. Pharm. Sci.*, 2015, **66**, 173–183.
22 D. Desai, J. Zhang, J. Sandholm, J. Lehtimäki, T. Grönroos, J. Tuomela and J. M. Rosenholm, *Mol. Pharmaceutics*, 2017, **14**, 3218–3227.
23 D. D. Mascolo, S. Varesano, R. Benelli, H. Mollica, A. Salis, M. R. Zocchi, P. Decuzzi and A. Poggi, *Cancers*, 2020, **12**, 104.
24 X. Guan, Z. Guo, T. Wang, L. Lin, J. Chen, H. Tian and X. Chen, *Biomacromolecules*, 2017, **18**, 1342–1349.
25 W. L. Chen, S. D. Yang, F. Li, C. X. Qu, Y. Liu, Y. Wang, D. D. Wang and X. N. Zhang, *Acta Biomater.*, 2018, **81**, 219–230.
26 Y. Zhu, C. Chen, Z. Cao, S. Shen, L. Li, D. Li, J. Wang and X. Yang, *Theranostics*, 2019, **9**, 8312–8320.
27 H. Y. Yang, Y. Li and D. S. Lee, *Macromol. Rapid Commun.*, 2020, **41**, 2000106.
28 C. C. Hung, W. C. Huang, Y. W. Lin, T. W. Yu, H. H. Chen, S. C. Lin, W. H. Chiang and H. C. Chiu, *Theranostics*, 2016, **6**, 302–317.
29 S. C. Liao, C. W. Ting and W. H. Chiang, *J. Colloid Interface Sci.*, 2020, **561**, 11–22.
30 C. Ding, J. Gu, X. Qu and Z. Yang, *Bioconjugate Chem.*, 2009, **20**, 1163–1170.
31 C. Wang, W. Yuan, F. Xiao, Y. Gan, X. Zhao, Z. Zhai, X. Zhao, C. Zhao, P. Cui, T. Jin, X. Chen and X. Zhang, *Front. Pharmacol.*, 2017, **8**, 572.
32 K. Liu, X. Wang, W. Fan, Q. Zhu, J. Yang, J. Gao and S. Gao, *Int. J. Nanomed.*, 2012, **7**, 1149–1162.
33 Q. Zhou, L. Zhang, T. H. Yang and H. Wu, *Int. J. Nanomed.*, 2018, **13**, 2921–2942.
34 Z. Yang, N. Sun, R. Cheng, C. Zhao, Z. Liu, X. Li, J. Liu and Z. Tian, *Biomaterials*, 2017, **147**, 53–67.
35 H. K. Makadia and S. J. Siegel, *Polymers*, 2011, **3**, 1377–1397.
36 E. M. Elmowafy, M. Tiboni and M. E. Soliman, *J. Pharm. Invest.*, 2019, **49**, 347–380.
37 M. Xu, C. Y. Zhang, J. Wu, H. Zhou, R. Bai, Z. Shen, F. Deng, Y. Liu and J. Liu, *ACS Appl. Mater. Interfaces*, 2019, **11**, 5701–5713.
38 J. Condeelis and J. W. Pollard, *Cell*, 2006, **124**, 263–266.
39 J. W. Pollard, *Nat. Rev. Cancer*, 2004, **4**, 71–78.
40 Y. Hattori, K. Shibuya, K. Kojima, A. Miatmoko, K. Kawano, K. Ozaki and E. Yonemochi, *Int. J. Oncol.*, 2015, **47**, 211–219.

 This journal is © The Royal Society of Chemistry 2022